Optomechanical Nonlinearity in Dual-Nanoweb Structure Suspended Inside Capillary Fiber

A. Butsch,[1,*] M. S. Kang,[1] T. G. Euser,[1] J. R. Koehler,[1] S. Rammler,[1] R. Keding,[1] and P. St.J. Russell[1,2]

[1]*Max Planck Institute for the Science of Light, Guenther-Scharowsky-Strasse 1, 91058 Erlangen, Germany*
[2]*Department of Physics, University of Erlangen-Nuremberg, 91058 Erlangen, Germany*

A novel kind of nanostructured optical fiber, displaying an extremely high and optically broadband optomechanical nonlinearity, is presented. It comprises two closely spaced ultrathin glass membranes (webs) suspended in air and attached to the inner walls of a glass fiber capillary. Light guided in this dual-web structure can exert attractive or repulsive pressure on the webs, causing them to be pushed together or pulled apart. The elastic deflection of the webs is, in turn, coupled to the electromagnetic field distribution and results in a change in the effective refractive index within the fiber. Employing a pump-probe technique in an interferometric setup, optomechanically induced refractive index changes more than 10^4 times larger than the Kerr effect are detected. Theoretical estimates of the optomechanical nonlinearity agree well with the experimental results. The dual-web fiber combines the sensitivity of a microoptomechanical device with the versatility of an optical fiber and could trigger new developments in the fields of nonlinear optics, optical metrology, and sensing.

Introduction.—Optical forces can originate from axial transfer of photon momentum or a transverse gradient in a propagating electromagnetic field. Classical by nature, they are closely related to the Casimir force of quantum electrodynamics [1–3] and are involved in a variety of light-matter interactions. The coupling of optical and mechanical degrees of freedom by radiation pressure inside high-finesse optical cavities is the founding principle behind the growing field of cavity optomechanics [4]. Attractive and repulsive optical gradient forces have been predicted and theoretically studied in coupled dielectric waveguide systems [5–8]. Recently the silicon-on-insulator platform has been used to demonstrate and explore a number of different optomechanical devices [9–12].

Low-loss microstructured optical fibers [13] offer the possibility of enhancing light-matter interactions through tight field confinement and propagation lengths of many meters. Examples include optoacoustic nonlinearities [14] and particle trapping and acceleration [15]. In a recent theoretical study, strong optomechanical nonlinearities, leading to transverse self-trapping of optical modes, were predicted to occur in a new type of microstructured optical fiber—the "dual-web" fiber [16].

Here we report both the successful fabrication of a guiding fused silica dual-web fiber and the experimental observation of its optomechanical nonlinearity. The nanowebs act as a pair of coupled optical waveguides, supporting even and odd optical eigenmodes, and when light is launched into them, optical gradient forces cause the webs to bend inward or outward depending on the symmetry of the optical mode [5]. This mechanical deflection causes the effective refractive index of the guided mode to increase, resulting in a power-dependent refractive index—an

optomechanical analogue of the Kerr effect [8,16]. In contrast to cavity-based [11] or photonic crystal [12] structures, the effect does not require an optical resonance and so is optically broadband. In addition, the nonlinearity can be further enhanced by driving the nanowebs at mechanical resonance. Unlike silicon-based optomechanical microdevices, the dual-web fiber offers the advantage of very long effective interaction lengths, permitting the nonlinear phase change to accumulate to a large value.

Experimental setup.—The dual-web fiber was drawn from fused silica capillaries by adapting the stack-and-draw process previously used to make single nanoweb fibers [17,18]. Figure 1(a) shows a scanning electron micrograph of the fiber microstructure. Two parallel silica nanowebs ~440 nm thick and 22 μm wide, separated by a ~550 nm air gap, are suspended inside a thick-walled fiber capillary [Fig. 1(c)]. An optical micrograph of the near field emerging from the fiber end face is shown in Fig. 1(b). The transmission power loss in the dual-web waveguide, measured using the standard cutback technique, was 35 dB/m (exponential decay rate $\alpha = 8.1 \text{ m}^{-1}$) at 1550 nm. Near- and far-field images of the light emerging from the fiber suggest that predominantly the even fundamental optical mode is excited. Although the first higher-order mode (with odd symmetry) is supported by the structure, its excitation can be suppressed by careful alignment of the launch to ensure that the phase across the webs is constant. Experimentally we found that the use of a lens with a numerical aperture (NA) of 0.6 also helped suppress the higher-order mode, which has an estimated NA (in the direction perpendicular to the web plane) of 0.7 compared to 0.5 for the even fundamental mode.

To detect nonlinear phase changes, the fiber sample was placed in one arm of an actively stabilized Mach-Zehnder
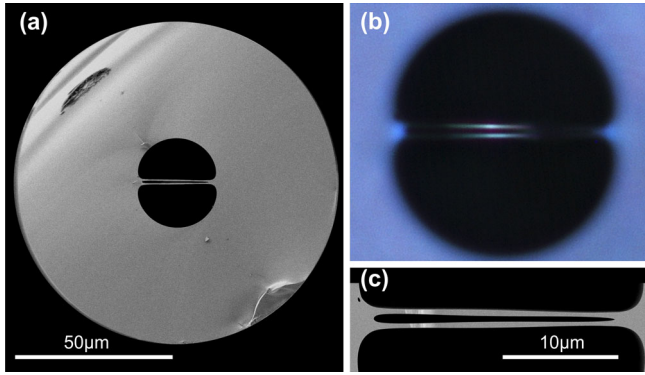
FIG. 1 (color online).   (a) Scanning electron micrograph of the dual-nanoweb fiber cross section (outer diameter 100 μm). (b) Near-field optical micrograph of the light emerging from the fiber end face when white light is launched into the core. (c) Detail of the core region; the two nanowebs are $\sim$440 nm thick and 22 μm wide, and the air gap is $\sim$550 nm wide.

(MZ) interferometer [Fig. 2(a)]. A sinusoidal amplitude-modulated pump wave with tunable frequency was used to optomechanically excite vibrations in the nanowebs. As mentioned above, the effective refractive index of the guided mode changes with nanoweb spacing. A weak probe beam at a slightly different wavelength can then retrieve the cumulative phase change along the fiber. Polarizers were used to control the polarization state in the sample and reference arms. At the output of the interferometer, the interfering beams were spatially overlapped by coupling to a single-mode fiber (SMF), followed by a fiber-coupled tunable bandpass filter that allowed selection of pump or probe signal before transmission to a photodiode. A feedback system, programmed in LABVIEW (3 dB roll-off frequency 10 Hz) with a piezo-mounted mirror and a detector at the interferometer output, was used to adjust and stabilize the MZ interferometer at quadrature, so as to ensure maximum phase sensitivity at the probe wavelength.

When the nanowebs begin to oscillate, driven by the modulated pump beam, the induced refractive index variation results in a phase change in the sample arm. The normalized amplitude $\hat{S}_m$ of the modulated probe signal (defined below), and its phase delay $\psi_{\rm OM}$ with respect to the modulated pump, can be determined by monitoring the signal at the interferometer output. Figure 2(b) illustrates a typical output signal (monitored by an oscilloscope) when the system is driven at resonance.

Pump (1550 nm) and probe (1543 nm) beams, polarized perpendicular to the plane of the webs (TM polarization), were launched into a sample of length $L = 97$ mm, yielding an effective length of $L_{\rm eff} = (1 - e^{-\alpha L})/\alpha = 67$ mm. The interferometer was balanced, using a combination of $\lambda/2$-plate and polarizer in each arm, so that the signals from the sample and reference arms were copolarized and had equal amplitudes at the second beam splitter, i.e., $|s_r| = |s_s|$ in Fig. 2(a).
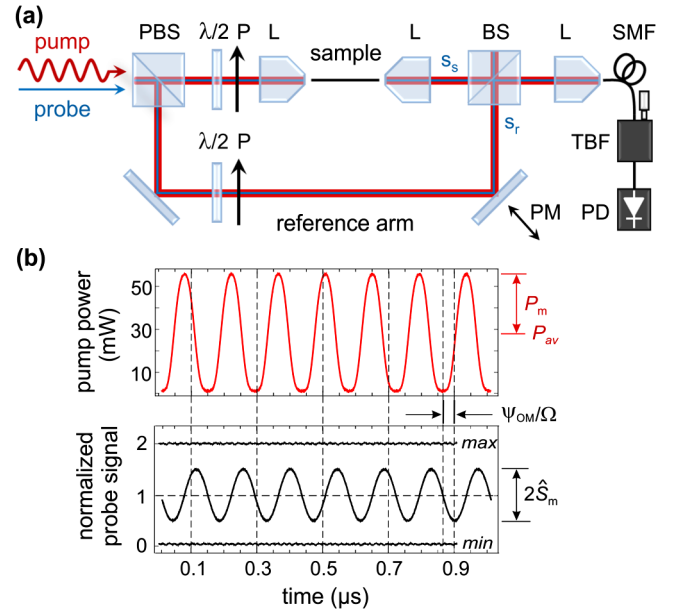
FIG. 2 (color online).   (a) Experimental setup: linearly polarized amplitude-modulated pump and a coaligned continuous-wave probe wave at a different wavelength are coupled into a Mach-Zehnder (MZ) interferometer. (P)BS: (polarizing) beam splitter, P: polarizer, L: lens, SMF: single-mode fiber, TBF: tunable bandpass filter, PD: photodiode, and PM: piezo-driven mirror. (b) Normalized probe signal at the interferometer output (lower), modulated at the resonant frequency of the dual-web (7.0 MHz). Maximum and minimum of the interferometer response correspond to zero and π phase difference between the arms. The red (upper) curve in (b) represents the driving pump wave with modulation amplitude $P_m = 28$ mW. The phase delay between pump and the probe waves is $\psi_{\rm OM}$.

Theory.—The modulated component $S(t)$ of the measured signal power at the output of the MZ interferometer, at quadrature and normalized to half the total power leaving the second beam splitter, takes the form

$$\hat{S}(t) = \frac{S(t)}{\frac{1}{2}(|s_s|^2 + |s_r|^2)} = \sin(\phi_0 \sin\Omega t) \approx 2{\rm J}_1(\phi_0)\sin\Omega t$$
$$= \hat{S}_m \sin\Omega t, \tag{1}$$

where only the first frequency sideband is considered in the Bessel function expansion. As a result, the amplitude of the sinusoidally modulated phase is given by $\phi_0 = {\rm J}_1^{-1}(\hat{S}_m/2)$. Assuming that the launched pump power in the sample is modulated as $P(t) = P_{\rm av} + P_m \sin\Omega t$, the modulated component of the cumulative phase change may be written

$$\frac{\phi(t)}{\sin\Omega t} = \gamma_{\rm OM} L_{\rm eff} P_m = \phi_0 = {\rm J}_1^{-1}(\hat{S}_m/2), \tag{2}$$

yielding

$$\gamma_{\rm OM}(\Omega) = \frac{1}{P_m L_{\rm eff}} {\rm J}_1^{-1}[\hat{S}_m(\Omega)/2], \tag{3}$$

where, for a series of Lorentzian resonances (the structure exhibits multiple eigenfrequencies as will be shown in the next section, where finite element modeling is used), the amplitude and phase of $\bar{\gamma}_{OM}(\Omega)$ relative to the sinusoidal pump can be written

$$\bar{\gamma}_{OM}(\Omega) = \sum_i \frac{\gamma_{OM}^i(0)}{1 - (\Omega/\Omega_{0i})^2 + iQ_i^{-1}(\Omega/\Omega_{0i})}$$

$$\gamma_{OM}(\Omega) = |\bar{\gamma}_{OM}(\Omega)|, \qquad \psi_{OM}(\Omega) = \arg[\bar{\gamma}_{OM}(\Omega)],$$

(4)

where Ω_{0i} is the resonant frequency (in rad/s), Q_i the quality factor, and $\gamma_{OM}^i(0)$ the nonlinear coefficient of the i-th resonance at zero frequency.

Results.—Figure 3(a) shows the measured response of the dual-web fiber as a function of drive frequency $f = \Omega/(2\pi)$. A strong resonance is seen at 7.0 MHz, two further weaker peaks being visible at 30 and 68.2 MHz. To clarify the origin of these peaks, the mechanical resonances were modeled using a finite element approach based on a scanning electron micrograph and the elastic parameters of fused silica [19]. The results [Fig. 3(b)] show that the upper and lower webs have nondegenerate resonant frequencies due to slight structural asymmetry,

(a)
(b)
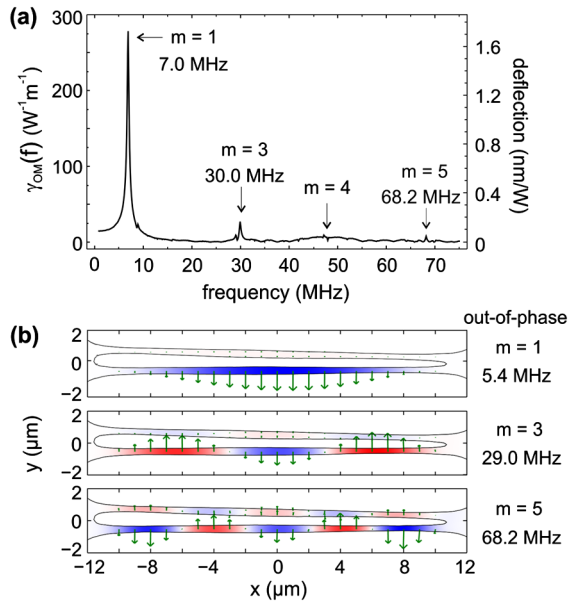
FIG. 3 (color online). (a) Nonlinear optomechanical coefficient as a function of drive frequency, showing higher-order mechanical resonances, measured for $P_m = 49$ mW. The corresponding deflection amplitude of the nanoweb per watt of power modulation can be read out using the scale to the right. (b) Finite element modeling: modes with one, three, and five lobes exist for which the webs oscillate out-of-phase in the vicinity of the optical mode. The motion of the lower web dominates, the upper web only playing a minor role. We attribute the mismatch between modeled and experimental resonant frequencies to tension in the webs, created during the drawing process.

but that nevertheless there is a degree of mechanical coupling between them. The mechanical resonances can be classified according to the number m of oscillating lobes along the web. Note that only the odd-order mechanical resonances are included in Fig. 3(b). This is because optical gradient forces cause either attraction or repulsion of the webs, depending on the symmetry of the optical modes [5]. As a consequence, acoustic modes with odd symmetry (i.e., webs oscillating out-of-phase) and an odd number of oscillating lobes ($m = 1, 3, 5$) are preferentially excited in the experiment, whereas even modes (webs oscillating in-phase) and those with an even number of lobes ($m = 2, 4$) are largely suppressed because their overlap integral with the fundamental optical mode (zero in a perfectly symmetric structure) is small.

The mismatch between the modeled (5.35 MHz) and measured (7.0 MHz) frequencies of the $m = 1$ resonance we attribute to frozen-in tension in the webs, created as the fiber rapidly cools to room temperature after being drawn. This will cause an increase in the resonant frequency, akin to the tuning of a stringed instrument. Following the analysis in [20], the eigenfrequencies of a plate of width b with clamped edges (length $L \gg b$) can be written as

$$f_m = \frac{1}{2\pi} \sqrt{\frac{1}{\rho w} \left[D\left(\frac{\pi(m + 1/2)}{b}\right)^4 + T\left(\frac{\pi(m + 1/2)}{b}\right)^2 \right]},$$

(5)

where ρ is the density, w the plate thickness, T the tension per unit width, and the flexural rigidity D is defined as $Ew^3/[12(1 - \nu^2)]$, where E is Young's modulus and ν is Poisson's ratio. Taking the values $\rho = 2203$ kg/m^3, $E = 72.5 \times 10^9$ N/m^2, $\nu = 0.17$, $b = 22$ μm, and $w = 0.44$ μm, the fundamental ($m = 1$) frequency without tension is 5.4 MHz. Applying tension of $T = 16$ N/m raises the resonant frequency to 7.0 MHz.

The tension-induced frequency mismatch gets smaller for higher-order modes, as expected from the theory, and indeed the modeled frequency of the $m = 5$ resonance agrees well with experiment. After thermal annealing at 1160 °C for 5 hours to release the tension, the frequency of the $m = 1$ resonance fell by more than 1 MHz, confirming that tension does indeed play a role.

Optomechanical response.—Figure 4(a) shows the dependence of γ_{OM} and ψ_{OM} on the drive frequency f at a launched pump power of $P_m = 28$ mW, measured in the vicinity of the 7 MHz resonance. The phase Ψ_{OM} varies from zero well below the mechanical resonance frequency (i.e., in the quasistatic regime when the web deflection is in-phase with the drive signal) to $\psi_{OM} = -\pi/2$ at resonance and $\Psi_{OM} = -\pi$ well above resonance, as expected of a driven harmonic oscillator.

Fitting these response curves to Eq. (4) yields $Q = 20.6$, $\gamma_{OM}(f_0) = 294$ W^{-1} m^{-1} (corresponding to $\phi_0 = 0.545$ rad), and $\gamma_{OM}(0) = \gamma_{OM}(f_0)/Q = 14.3$ W^{-1} m^{-1}
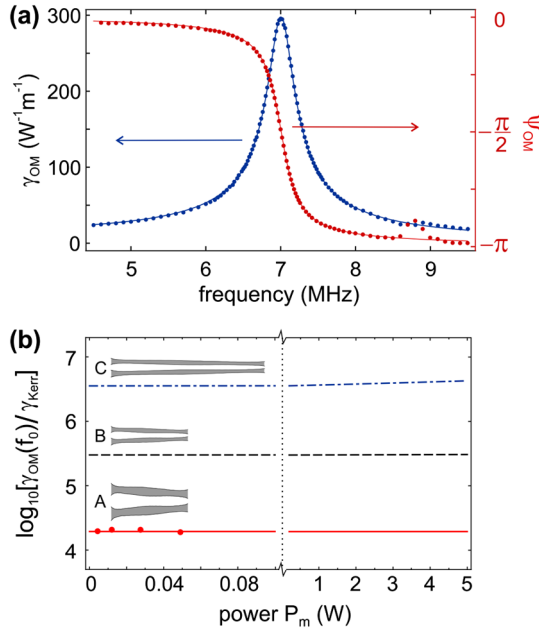
FIG. 4 (color online). (a) Frequency response of γ_{OM} (blue) and ψ_{OM} (red) in the vicinity of the resonance at 7.0 MHz. The dots are the measured values and the full lines are a fit to a single Lorentzian resonance. (b) The ratio of the resonant nonlinear optomechanical coefficient $\gamma_{OM}(f_0)$ to the effective Kerr coefficient γ_{Kerr} as a function of power calculated for three different structures. A: the actual dual-web structure as shown in Fig. 1; B: the same structure scaled by 1/2 perpendicular to the webs; and C: structure B stretched horizontally by a factor of 2. The dots show the measured $\gamma_{OM}(f_0)$ values for $P_m = 4, 12, 28$, and 49 mW.

($\phi_0 = 26.5$ mrad). The nonlinear coefficient based solely on the Kerr effect γ_{Kerr} is calculated using the nonlinear refractive index of silica and the effective nonlinear mode area [21]. Its value in the experimental dual-web structure is ~ 0.014 W^{-1}m^{-1} (for comparison γ_{Kerr} for an air-silica photonic crystal fiber with a 1 μm glass core is ~ 0.2 W^{-1}m^{-1} [13]). Thus the nonresonant optomechanical nonlinearity $\gamma_{OM}(0)$ is ~ 1000 times larger than γ_{Kerr}, and $\gamma_{OM}(f_0)$ at resonance is 20 000 times larger.

Additionally the γ_{OM} coefficient can be calculated employing the theoretical approach presented in [16]. The results, based on a full model taking account of the exact structure, are 13.8 W^{-1}m^{-1} for the nonresonant and 284 W^{-1}m^{-1} for the resonant case, agreeing well with the experimental data.

In Fig. 4(b) the ratio $\gamma_{OM}(f_0)/\gamma_{Kerr}$, calculated for the structure used in the experiment, is plotted against the drive power amplitude P_m (red solid line), and the measured values are shown at $P_m = 4, 12, 28$, and 49 mW (dots). The γ_{OM} value remains nearly constant as the drive power increases. In contrast to the planar structure theoretically treated in [16], the experimental dual-web structure exhibits a slight convex thickness profile along the webs, so that the optical mode can be well localized even at low powers

[Fig. 1(b)]. When the power is increased, deflections of the order of some nanometers can be obtained at resonance [see Fig. 3(a)], but the optical mode distribution does not change significantly so that the dependence of the modal index on drive power remains linear. The optomechanical response can be further enhanced by making the structure more flexible, e.g., by reducing the thickness of the webs and bringing them closer together (the optically induced pressure falls exponentially with increasing web spacing [7]). This can be achieved during the drawing process by changing the fiber diameter and applied pressure. For example, when the actual structure is scaled by a factor 1/2 across the webs [structure B in Fig. 4(b)], the corresponding resonant γ_{OM} value (assuming that the Q factor remains constant) is ~ 2700 W^{-1}m^{-1}, while the Kerr coefficient is ~ 0.009 W^{-1}m^{-1}. As a result, the $\gamma_{OM}(f_0)/\gamma_{Kerr}$ ratio increases to $\sim 3 \times 10^5$ [dashed line in Fig. 4(b)]. The optomechanical response is enhanced further if structure B is stretched horizontally by a factor of 2 (structure C: $b \approx 44$ μm, $w \approx 0.22$ μm, and air-gap width $h \approx 0.28$ μm), so that $\gamma_{OM}(f_0)$ is $\sim 2.4 \times 10^4$ W^{-1}m^{-1} and $\gamma_{Kerr} \approx 0.007$ W^{-1}m^{-1} yielding a ratio of $\sim 3.5 \times 10^6$ at drive powers in the milliwatt range and showing a steady linear increase with power as expected of a strong optomechanical nonlinearity [16] [dash-dotted line in Fig. 4(b)].

In conclusion, dual-nanoweb silica fibers can be fabricated that yield very strong optomechanical nonlinearities. By optimizing the structural parameters, such as web thickness, separation, and width, the optomechanical response can be further enhanced, perhaps eventually leading to formation of self-channelled guided beams as predicted in [16]. In addition, this kind of optomechanical fiber provides a new platform for sensing (e.g., as a high-bandwidth dynamic or ultrasensitive static pressure sensor) and nonlinear optics (power-dependent zero-dispersion wavelengths).

*Corresponding author.
anna.butsch@mpl.mpg.de

[1] H. B. G. Casimir and D. Polder, Phys. Rev. **73**, 360 (1948).
[2] S. K. Lamoreaux, Phys. Rev. Lett. **78**, 5 (1997).
[3] J. N. Munday, F. Capasso, and V. A. Parsegian, Nature (London) **457**, 170 (2009).
[4] T. J. Kippenberg and K. Vahala, Science **321**, 1172 (2008).
[5] M. L. Povinelli, M. Loncar, M. Ibanescu, E. J. Smythe, S. G. Johnson, F. Capasso, and J. D. Joannopoulos, Opt. Lett. **30**, 3042 (2005).
[6] A. Mizrahi and L. Schaechter, Opt. Lett. **32**, 692 (2007).
[7] F. Riboli, A. Recati, M. Antezza, and I. Carusotto, Eur. Phys. J. D **46**, 157 (2008).

[8] W. H. P. Pernice, M. Li, and H. X. Tang, Appl. Phys. Lett. **95**, 123507 (2009).

[9] M. Li, W. H. P. Pernice, C. Xiong, T. Baehr-Jones, M. Hochberg, and H. X. Tang, Nature (London) **456**, 480 (2008).

[10] M. Li, W. H. P. Pernice, and H. X. Tang, Nature Photon. **3**, 464 (2009).

[11] G. S. Wiederhecker, L. Chen, A. Gondarenko, and M. Lipson, Nature (London) **462**, 633 (2009).

[12] M. Eichenfield, R. Camacho, J. Chan, K. J. Vahala, and O. Painter, Nature (London) **459**, 550 (2009).

[13] P. St.J. Russell, J. Lightwave Technol. **24**, 4729 (2006).

[14] M. S. Kang, A. Brenn, and P. St.J. Russell, Phys. Rev. Lett. **105**, 153901 (2010).

[15] O. A. Schmidt, M. K. Garbos, T. G. Euser, and P. St.J. Russell, Opt. Lett. **37**, 91 (2012).

[16] A. Butsch, C. Conti, F. Biancalana, and P. St.J. Russell, Phys. Rev. Lett. **108**, 093903 (2012).

[17] P. V. Kaiser and H. W. Astle, Bell Syst. Tech. J. **53**, 1021 (1974).

[18] N. Y. Joly, T. A. Birks, A. Yulin, J. C. Knight, and P. St.J. Russell, Opt. Lett. **30**, 2469 (2005).

[19] P. J. Thomas, N. L. Rowell, H. M. van Driel, and G. I. Stegeman, Phys. Rev. B **19**, 4986 (1979).

[20] M. C. Weinberg, B. T. Cunningham, and C. W. Clapp, J. Microelectromech. Syst. **9**, 370 (2000).

[21] J. Lægsgaard, N. A. Mortensen, J. Riishede, and A. Bjarklev, J. Opt. Soc. Am. B **20**, 2046 (2003).